ZIBELINE INTERNATIONAL™ PUBLISHING

ISSN: 2716-7100 (Online)
CODEN: MCEMC2

Materials & Corrosion Engineering Management (MACEM)

DOI: http://doi.org/10.7508/macem.01.2024.25.39

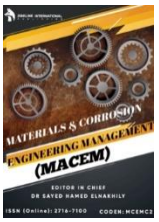

RESEARCH ARTICLE

EXPLORING ALUMINUM CORROSION IN HYDROCHLORIC ACID: EFFECTS OF ZINC OXIDE NANOPARTICLES AND PLANTAIN PEEL EXTRACT AS INHIBITORS

Olatunji Peace OluwanifemI[a*], Korode Temitayo Bukola[b], Akpeji Bamidele Honesty[c]

[a]*Department of Chemical Engineering, Federal University of Petroleum Resources, Effurun, Delta state.*
[b]*Petroleum and Natural Gas Processing Department, Petroleum Training Institute, Effurun, Delta State.*
[c]*Department of Chemistry, Federal University of Petroleum Resources, P.M.B 1221, Effurun, Delta State, Nigeria.*
[*]*Corresponding Author Email: bukola.korode@yahoo.com*

ARTICLE DETAILS

Article History:

Received 12 March 2024
Accepted 14 April 2024
Revised 18 May 2024
Available online 07 June 2024

ABSTRACT

This study investigates the corrosion behavior of aluminum in hydrochloric acid (HCl) solutions, exploring the efficacy of zinc oxide nanoparticles and plantain peel extract as inhibitors. Through weight loss analysis, factors such as adsorption, kinetics, thermodynamics, corrosion rate, and inhibitor efficiency were examined. Optimal inhibition efficiency of 46.70% was achieved at 303K with 500 ppm inhibitor concentration in 0.5M HCl. Adsorption parameters aligned with Langmuir isotherm, indicating strong correlation (R2 ≈ 0.9999). Activation energy and free energy values suggested an endothermic reaction. Zinc oxide nanoparticles, in conjunction with plantain peel extract, exhibited effective corrosion inhibition. The study underscores the role of flavonoids, saponin, alkaloids, proteins, and tannins in facilitating bio-reduction of zinc acetate into nanoparticles. Further research avenues include exploring alternative corrosion analysis techniques and optimizing corrosion control processes.

KEYWORDS

corrosion, nanoparticles, inhibitory efficiencies, kinetic

1. INTRODUCTION

According to a study, corrosion-related expenses account for a small portion of the GDP of the world's most developed countries, often less than that allocated to public healthcare or education (Palou et al., 2014). Corrosion and related processes have always piqued scientists' interest. Natural events such as corrosion can weaken the properties of metals and alloys, rendering them ineffective (Ennouri et al., 2017). Aluminum is a strong, lightweight, malleable metal that is non-magnetic and non-sparkling, depending on the degree of surface roughness. It is exceptionally smooth. El-Etre describes its appearance as varying from dull gray to silvery (El-Etre, 2003). Aluminum and its alloys can be used in a wide range of hazardous environments and industries, including construction and interior fittings. Aluminum is known for its low density and partial resistance to corrosion due to passivation; however, it corrodes in acidic aqueous environments. Extensive research has been conducted on the corrosion of aluminum and its alloys in acidic environments (Muller, 2002). Ionic aluminum is found in all naturally occurring fluids as well as the tissues of most animals and plants (Jiang et al., 2008). It is the third most common element and the most abundant metal in the earth's crust, accounting for approximately 8% of all mineral components (Verstraeten et al., 2008). Despite its widespread consumption, aluminum in food occurs in trace amounts, indicating that healthy people are not seriously threatened by it (Proudfoot, 2009). The most important property of aluminum is its high strength-to-weight ratio. Aluminum is a popular material for use in a variety of applications due to its excellent thermal and electrical conductivity and low cost (Davis et al., 1999). The mechanical properties of pure aluminum can be significantly enhanced by the formation of alloys. Several alloy series have been produced. The composition and concentration of the constituents affect the mechanical properties and corrosion resistance of aluminum alloys. The alloy's purity determines its resistance to pitting corrosion. Therefore, it is essential to comprehend the chemical composition of the aluminum alloy.

The industry employs a variety of compounds as corrosion inhibitors to prevent or reduce metal corrosion in acidic environments. Given the toxicity and high cost of these compounds, it is critical to identify less hazardous and more expensive inhibitors. As environmental awareness has grown and environmental regulations governing the use of man-made corrosion inhibitors have tightened, there has been a push for green corrosion inhibitors, also known as environmentally sustainable alternatives (Ryl et al., 2019). In addition to non-toxic man-made chemicals such as colors, rare earth elements, Schiff bases, and specific medications, natural plant-based materials can be used to create environmentally safe corrosion inhibitors (Oguzie, 2005; Haley, 1965; Ju et al., 2008; Raghavendra and Bhat, 2018; Chaubey et al., 2017). Scientists have spent over 20 years developing novel, non-toxic aluminum corrosion inhibitors (Xhanari et al., 2017).

Several theories have been proposed to explain why alkaline aqueous conditions inhibit green corrosion in aluminum and its alloys. Green corrosion inhibitors are thought to slow aluminum corrosion by decreasing reactive reagent diffusion speeds to and from the metal's surface, increasing the pH stability spectrum of amphoteric layers composed of aluminum oxides and hydroxides, strengthening or rebuilding weakened oxide and hydroxide layers, and/or removing corrosion products from the metal's surface (Mansfeld, 1987). Bee products have been described as effective green corrosion inhibitors for aluminium and its alloys. Natural honey's anti-corrosive properties are investigated when exposed to an Al-Mg-Si alloy in seawater (Rosliza et al., 2010). SEM analysis confirmed the presence of a thin layer of corrosion inhibitor on the protected alloy's surface, which slowed overall corrosion.

A group researcher reported similar findings (Gudic et al., 2016). Natural products made from tannin-rich plant extracts, extracts from various plant

Quick Response Code	Access this article online	
	Website: www.macej.com.my	DOI: 10.26480/macem.01.2024.25.39

parts such as leaves and roots, mint, Lawsonia, and Opuntia extract (Rahim et al., 2008; Noor, 2009; Okafor et al., 2010; Bedair et al., 2015; El-Etre et al., 2005; El-Elte, 2003). A group researcher investigated the effects of natural materials, including mint leaves and stems, on mild steel corrosion in 1.0 M HCl (Bedair et al., 2015). They concluded that the plant extracts were mixed-type inhibitors. To improve their inhibitory efficiencies, the quantities of these compounds were increased while the ambient temperature was lowered. Nonetheless, there has been little, if any, research into the numerical modeling of the molecular structure properties of mint- and honey-friendly inhibitors as HCl-soluble aluminum corrosion inhibitors. Several articles have mentioned using mint or honey as a corrosion inhibitor. Thus, the authors concentrated on evaluating honey and mint as inhibitors of aluminum corrosion in HCl using numerical models of molecular structures and then theoretically confirming using two relatively simple techniques, gravimetric and gasometric. As a result, the purpose of this study is to investigate aluminum corrosion in hydrochloric acid and the effects of zinc oxide nanoparticles and plantain peel extract as inhibitors.

2. Related Literature

The degradation of a metal caused by a chemical reaction between it and the environment is known as corrosion (Eugene Uwiringiyimana et al., 2016). The form and rate of deterioration are determined by the type of metal used as well as environmental factors, notably gases that come into contact with the metal (Terence, 2019). The discipline of corrosion engineering is focused on preventing and controlling corrosion. In its most widespread usage, this term refers to the electrochemical oxidation of metal in response to an oxidant like oxygen or sulfate. An example of electrochemical corrosion that is well-known is rusting, which is the development of iron oxides. This kind of damage often results in oxides or salts of the parent metal, which give the material a recognizable orange color. A study on the influence of various peel extracts on the corrosion behavior of aluminum alloys in an alkaline medium (Namrata et al., 2015).

Utilizing weight loss, electrochemical impedance spectroscopy (EIS), linear polarization, and potentiodynamic polarization techniques, three peels' ability to inhibit aluminum alloy (AA) in a 1 M NaOH solution was examined. The peels are Pisum sativum (PqS), Solanum tuberosum (ST), and Citrus reticulata (CR) (Tafel). These three peel extracts were discovered to perform extremely well on AA in an alkaline medium. At 1.5 g/L, PS showed a maximal inhibition efficiency (g%) of 94.5%. Atomic force microscopy (AFM) and scanning electron microscopy (SEM) were used to examine the effectiveness of AA protection in blocked systems (AFM). The Langmuir adsorption isotherm was followed when inhibitors were adsorbed on the surface of AA. Potentiodynamic polarization experiments revealed that all of the inhibitors inhibited corrosion in a mixed mode. SEM and AFM results combined well with electrochemical and weight loss study results.

The pitting corrosion of 430 stainless steel is inhibited by benzyl triethyl ammonium chloride (BTEAC) (Devi and Selvarani, 2014). They used mass loss as a way to analyze electrochemical behavior in their experiment, which was carried out in 1 M HCl. Because N ions and electrons in BTEAC's molecule are adsorbed on the metal surface, it has been shown to be a successful inhibitor (Bentiss et al., 2012). In relation to the weight loss investigation, they discovered that when BTEAC concentrations in 1 M HCl rise, the rate of stainless-steel deterioration declines. In this experiment, the 430 stainless steel type in 1M HCl with BTEAC addition at 303 and 313K was compared. According to research, BTEAC's efficacy dropped with increasing temperature (Idris et al., 2013). The effectiveness of an inhibitor's inhibition increases with an increase in the inhibitor's concentration, according to research published (Rahuma et al., 2014; James et al., 2014; Mhammedi and Chaini, 2007; 2011).

This research looked at the effect of pyrazolo (3, 4-b) pyridine on stainless steel corrosion in 1 M HCl solutions in order to understand the electrochemical behavior of stainless steels. This was accomplished using potentiodynamic polarization, electrochemical impedance spectroscopy, and the weight loss method. Another study by used the weight loss method in a 0.5 M solution of hydrochloric acid to determine the effectiveness of the inhibitor; the results showed that Pyrazolo (3, 4-b) Pyridine prevents weight loss of stainless steel because the inhibitor is adsorbed onto the metal's surface (Olawale et al., 2015). Hydrochloric acid showed the best inhibitory efficiency, which was 80.5%; after 336 hours of testing, it was concluded that cashew waste is an effective corrosion inhibitor because it will lower import costs, increase the nation's GDP, and remove harmful chemical inhibitors from the environment.

The use of environmentally friendly materials as corrosion inhibitors for aluminum in hydrochloric acid (HCl) using both density functional theory (DFT) at the B3LYP/6-31G* basis set level and semi-empirical methods is also explored in a study on Environment-Friendly Corrosion Inhibitors for Aluminum in Hydrochloric Acid: Quantum and Experimental Research (AM1, PM3, MINDO, and RM1) (Tarek et al., 2022). Investigating their inhibition efficiency (%IE) in terms of their molecular structure is the goal of this work. The highest occupied molecular orbital energy (EHOMO) and lowest unoccupied molecular orbital energy (ELUMO) have been computed, along with other quantum chemical parameters such as the energy gap (DE), charge on the reactive core, hardness (h), and total energy. Using the MINDO method, the electronic energies and charge densities of the inhibitors in use were determined.

Theoretical computations were also performed, and the outcomes demonstrated a strong correlation with the experimental findings. Using gravimetry and gasometry measurements, the effects of honey and mint on aluminum corrosion were investigated in a 1.0 M hydrochloric acid (HCl) solution. In acid solutions, it was discovered that honey and mint were both effective inhibitors of aluminum corrosion, with honey being the more favorable option. The inhibitory impact of the used inhibitors was addressed due to the adsorption of their components on aluminum surfaces. Because honey has a higher dipole moment than mint, honey adheres to aluminum surfaces more effectively. Gravimetry and gasometry yield nearly identical IE readings.

3. Materials and Methods

Materials and methods used for this study are stated below:

3.1 Experimental Analysis

For this study, aluminum was gotten from any available fabricating or fitting store, and the unripe plantain peel was gotten gotten from a local market both in Warri and Delta State. Materials used for this research are zinc oxide nanoparticles, unripe plantain peel extract (Musa paradisiaca), specific molar concentrations of hydrogen chloride (HCl), zinc acetate, distilled water, sodium hydroxide (NaOH), liquid soaps, ethanol, and acetone. Apparatus to be used are beakers, measuring cylinders, conical flasks, sieves, digital weighing balances, magnetic stirrer hot plates, laboratory ovens, water baths, metal files, brushes, threads, and aluminum coupons. The pretreatment of the sample was done by washing and drying the sample (unripe plantain peel) in an oven for 2-3 days and grinding it using an industrial grinder. The extract was characterized to determine its physical and chemical properties, such as protein, ash, yields, and solubility. Analysis for this study was done with Fourier transform infrared spectroscopy (FTIR) analysis and UV-Visible Spectroscopy.

3.2 Phytochemical Analysis

3.2.1 Test for Saponins

0.2g of extract was shaken with 5 ml of distilled water in a test tube. Frothing that persists on warming was taken as evidence for the presence of saponins (Odeja et al., 2015).

3.2.2 Test for Alkaloids

0.2g of extract was shaken with 1% HCl for two minutes. The mixture was filtered and drops of Wagner's reagent were added. The formation of a precipitate indicated the presence of alkaloids (Odeja et al., 2015).

3.2.3 Test for Phenols

0.2g of extracts were dissolved in a ferric chloride solution. A green or dirty green precipitate indicated the presence of phenolic compounds (Odeja et al., 2015).

3.2.4 Tests for Steroids (Salkowski's Test)

0.2g of the sample was dissolved in 2 ml of chloroform. Concentrated sulfuric acid was carefully added to form a lower layer. A reddish-brown color at the inter-phase indicated the deoxysugar characteristics of cardenolides (Odeja et al., 2015).

3.2.5 Test for Flavonoids

0.5g of magnesium powder and two drops of concentrated hydrochloric acid were added to 3 ml of the extracts. A red or intense red coloration indicated the presence of flavonones (Odeja et al., 2015).

3.2.6 Test for Anthraquinones

0.2g of the sample was shaken with 4 ml of benzene. The mixture was

filtered, and 2 ml of a 10% ammonia solution was added to the filtrate. The mixture was shaken, and the presence of a pink, red, or violet color in the ammoniacal (lower) phase indicated the presence of free anthraquinones (Odeja et al., 2015).

3.2.7 Test for Reducing Sugars

0.2 g of the pretreated sample was shaken with distilled water and filtered. The filtrate was boiled with drops of Fehling's solutions A and B for two minutes. An orange precipitate on boiling with Fehling's solution indicated the presence of reducing sugars (Odeja et al., 2015).

3.2.8 Test for Cardiac-Active Glycoside (Keller-Killani test)

0.2 g of the pretreated sample was dissolved in 2 ml of glacial acetic acid containing one drop of ferric chloride solution, followed by the addition of 1 ml of concentrated sulfuric acid. A brown ring at the interface confirmed the presence of cardiac glycoside (Odeja et al., 2015).

3.2.9 Test for Tannins

0.2g of the pretreated sample was stirred with distilled water and filtered. Ferric chloride was added to the filtrate. A blue-black, green, or blue-green precipitate was taken as evidence for the presence of tannins (Odeja et al., 2015).

3.2.10 Test for Phlobatannins

The pretreated sample (0.5g) was dissolved in distilled water and filtered. The filtrate was boiled with a 2% HCl solution. Red precipitate shows the presence of phlobatannins (Odeja et al., 2015).

3.2.11 Test for Glycosides

The extracts were hydrolyzed with HCl solution and neutralized with NaOH solution. A few drops of Fehling's solutions A and B were added. A red precipitate indicates the presence of glycosides (Odeja et al., 2015).

Extraction of plant-aided synthesis of ZnO nanoparticles from unripe plant peels (*Musa paradisiaca*)

3.3 Preparation of Plant Extract

The unripe plantain peels (*Musa paradisiaca*) were collected from Effurun market within the Warri community in Delta State, Nigeria. The peels were washed several times with distilled water to remove any debris or particulates carried along during the collection of peels, then air-dried at room temperature for 4 days. The plantain peels were then pulverized with a standard electric blender and sieved using a laboratory test sieve with an aperture of 550 mm. About 2 grams of dried pulverized peels were used in preparing the aqueous extract in 500 ml of distilled water and heated at 80 °C for about 1 hour. The extracting mixture displayed a color change in its aqueous solution from watery to dark brown. The extract was separated by filtration using the WhatmanTM filter paper and stored in polyethylene terephthalate (PET) bottles in order to be used for further synthesis of ZnO nanoparticles.

3.4 Preparation of 0.01M Zinc Actetate (Zn(CH3COO)2.2H2O)

The analytical-grade zinc acetate used in this synthesis was procured from Rovet Scientific Laboratories in Benin, Nigeria. A 0.01M solution of zinc acetate (CH3COO)2Zn2H2O was prepared by dissolving 2.195 g of zinc acetate in 1000 ml of distilled water.

3.5 Preparation of 1M NaOH

Similarly, a 1M solution of sodium hydroxide (NaOH) was prepared by weighing 40g of NaOH pellets and then dissolving them in 1000 ml of distilled water.

3.6 Synthesis of Zinc Oxide Nanoparticles (ZnONPs)

The procedure of extraction and synthesis is similar to the one described, but with some modifications (Haque et al., 2020; Elemike et al., 2021). In this synthesis procedure, 50 ml of the aqueous extract of the peels and 500 ml of 0.01M zinc acetate solution were mixed together at a ratio of 1:10, with an added volume of 20 ml of NaOH solution dropwise. The resulting mixture was then mixed by continuously stirring on a magnetic stirrer at a temperature of 70 ^{o}C for about 3 hours. During this reaction time, the color of the colloidal solution gradually changed from brown to a cream-colored solution, which was indicative of an increased rate of bioreduction of the zinc acetate and the formation of zinc hydroxide $Zn(OH)_2$ precipitate.

3.7 Purification of ZnONPs

The $Zn(OH)_2$ formed as precipitate was purified by washing with distilled water and then centrifuged at 7000 rpm. The supernatant was discarded, leaving a pure white precipitate of ZnONPs, which was dried in an LD-201-E Vision Scientific Drying oven at 70^{0}C in order to obtain the desired ZnO nanoparticles. The long procedure process is summarized in Figure 1.

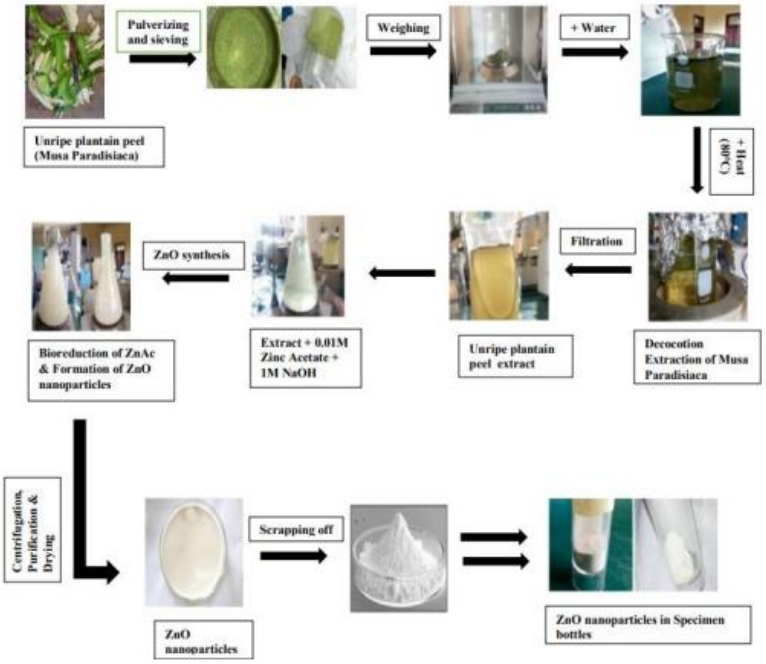

Figure 1: Process flow diagram for the preparation of Unripe Plantain (UP) peels & synthesis of UP-ZnO Nps.9 (Imade et al., 2022)

4. METHODOLOGY

Weight loss method was used in this study. The aluminum specimen will be cut into coupons of the required sizes (4 x 2 x 0.6) cm then will be abraded with a series of silicon carbide abrasive paper, washed in distilled, degreased with ethanol, dried with acetone, dried in the air, and weighed accurately. Aluminum specimens thereafter will be immersed in 100ml volume of a concentration (0.5M, 1.5M, 2.0M) of HCl in a beaker with and without addition of different concentrations of zinc oxide nanoparticles blended with unripe plantain peel extract. After some hour's interval at room temperature the aluminium specimens will be retrieved and dipped in distilled water, immersed in ethanol solution, scrubbed with a brush, to remove residual acids, and inhibitor and then be dried in acetone before reweighed, The weight loss data will be gained from the average value of

three parallel samples in 1.5M HCl with chitosan extract at different concentrations.

4.1 Determination of Inhibition Efficiency

The inhibition efficiency will be determined using equation 1

$$IE\ (\%) = \frac{W_1 - W_2}{W_1} \times 100 \quad (1)$$

Where, W1 = the weight loss in the absence of inhibitor

W2 = the weight loss in the presence of inhibitor

4.2 Determination of Corrosion Rate

Corrosion rate was determined using equation 2

$$\text{Corrosion rate (mmpy)} = \frac{kw}{ATD} \quad (2)$$

Where, k is a constant with value as 87.6mmpy, W is the weight loss (mg), A is the cross-sectional area (mm2), T is the time (hrs), D is the density (g/cm^3).

4.3 Determination of Surface Coverage

The degree of surface coverage was calculated from the weight loss measurement. Using equation 3

$$Surface\ coverage = \frac{W_A - W_P}{W_A} \quad (3)$$

Where, WA is the weight loss gotten from the absence of the inhibitor and Wp is the weight loss gotten in the presence of the inhibitor

4.4 Effect of Inhibitor Concentration

The effect of the concentration of the inhibitor on corrosion was investigated by changing the initial concentration of the inhibitor in the range 50ppm, 150ppm, 350ppm, 500ppm of 0.5M, 1.5M, 2.0M of HCl at room temperature for different days.

4.5 Effect of Immersion Time

The effect of exposure time on corrosion was observed for 5,10,15,20 hours in 100ml of inhibitor with 0.5M, 1.5M, 2.0M HCl concentration.

4.6 Effect of Temperature

The polished and pre-weighed specimens in duplicate was suspended in 100 mL of the test solution without and with the addition of different concentrations of the chitosan extract for 5hr in the temperature range of 40, 50, 60°C using the water bath

4.7 Thermodynamic Study

Thermodynamic parameters including entropy and enthalpy was calculated using transition state equation 4.

$$CR = \left(\frac{RT}{Nh}\right) EXP\left(\frac{\Delta S}{R}\right) \text{EXP}\left(\frac{-\Delta H}{RT}\right) \quad (4)$$

Where, CR = Corrosion rate,

h = Plank's constant $6.626176 \times 10^{-34}\ {}^{m^2 kg}/_{S}$

N =Avogadro's number ($6.02252 * 10^{23}$ mol^{-1})

R = Universal gas constant,

T = Absolute temperature.

Enthalpy (ΔH) = Slope X 2.302 X R

Entropy (ΔS) = 2.303 X R (Intercept – logR/Nh)

4.8 Kinetic Study

The temperature effect on aluminum corrosion rate was studied through 0.5, 1.5 & 2.0M of HCl in the absence and presence of Zinc oxide nanoparticles with a blend of musa paradisca extract at the temperature of 313–343 K. Activation parameters for the corrosion study will be estimated from an Arrhenius equation 5

$$K_{CR} = AExp\left|\frac{Ea}{RT}\right| \quad (5)$$

Where; KCR is corrosion rate, A is modified frequency factor (pre-exponential factor), Ea is activation energy ($KJmol^{-1}$), R is gas constant (8.314 $Jmol^{-1}$ K), and T is absolute temperature (K)

4.9 Half-Life Equation

The half-life of the inhibitor was determined using the equation as stated in equation 6

$$\text{In}\left({}^{W_f}/_{W_0}\right) = -kt \quad (6)$$

Where k is the half-life rate constant. The values were obtained from the slope of the graph of ln (Wf/W0) against exposure time at room temperature. The values for the half-life were calculated using equations 7 to 7.5.

$$t\frac{1}{2} = \frac{0.693}{k} \quad (7)$$

Zeroth order: $W_o = kt + \Delta W$ (7.1)

First order: $In = (W_o - \Delta W) = kt + In\ \Delta W$ (7.2)

Second order: $\frac{1}{Wa} = kt + \frac{1}{\Delta W}$ (7.3)

Pseudo first order: $\text{In} = (W_o - W_F) = InW_o - kt$ (7.4)

Pseudo Second order: $\frac{t}{wi} = \frac{k}{wo} + (\frac{1}{wf}) = InW_i - kt$ (7.5)

4.10 Adsorption Study

Molecular adsorption was used to further explain inhibition of corrosion. The surface charge and nature of metal, organic compounds chemical structures, types of aggressive media and molecule charge distribution are identified factor influencing process of adsorption.

4.11 Langmuir adsorption isotherm

$$\frac{c}{\emptyset} = \frac{1}{k} + C \quad (8)$$

Where; C is the inhibitor concentration, Ø is the degree of surface covered by the inhibitor, and K is the adsorption equilibrium constant gotten from a plot of C/Θ against C see equation (8). K is also related to the standard free energy of adsorption (ΔG). As using equation 6 (Nanna et al., 2014).

$$\Delta G = -RTIn\ (55.5 * K) \quad (9)$$

4.12 Temkin Adsorption Isotherm

According to Temkin adsorption isotherm, the degree of surface coverage (θ) is related to inhibitor concentration (C) as stated by equation 10.

$$\Theta = In\ C + In\ K \quad (10)$$

Where; Θ is a linear function of ln C, K is the adsorption equilibrium constant and C is the inhibitor concentration, (g/ml) (Fuchs – Godec et al., 2009). A plot of Θ against lnC will give a straight line plot, if Temkin isotherm is followed.

4.2 Freundlich Adsorption Isotherm.

The fitting of non – ideal system was done by fitting the experimental data to Freundlich adsorption isotherm (Yaro and Khadom, 2008). This is expressed in equation (11).

$$\theta = KC^n \quad (11)$$

Equation 12 can be re – written as;

$$In\theta = +\frac{n}{n}\ C \quad (12)$$

Where; θ is degree of surface coverage, k is equilibrium constant of adsorption, n is molecular interaction parameter

4.3 EL-Awady Adsorption Isotherma

The fitting of non – ideal system was done by fitting the experimental data

to EL-Awady adsorption isotherm (Yaro and Khadom, 2008). This is expressed in equation (13)

$$Log\frac{\theta}{1-\theta} = Log\ K + yLogC \quad (13)$$

Where; θ is degree of surface coverage, k is equilibrium constant of adsorption, n is molecular interaction parameter.

5. Results and Discussion

5.1 Results from the Experiment

Table 1 : Phytochemical Analysis of Musa paradisiaca Extract

Serial Number	Test Performed	Results
1	Total Volume of sample	29mls
2	Appearance	Liquid
3	Colour Description	Brown
4	Saponin	+
5	Reducing Sugars	+
6	Alkaloids	+
7	Protein (Amino acids)	+
8	Steroids	+
9	Tannins	+
10	Anthraquinones	-
11	Phenolic compounds	-
12	Carbohydrate	+
13	Terpenoids	-
14	Glycoside	+
15	Flavonoids	+

Keys: (+) indicates present, **(-)** indicates absent. A sound qualitative analysis test of phytochemical components was carried out on the musa paradisiaca extract. Qualitative determination can be seen from the change in colour. The presence of the tannins, flavonoids,and saponin showed that the Musa paradisiaca extract has potential to inhibit corrosion in hydrochloric acid

5.2 Fourier Transform from Infrared Spectroscopy (FTIRs) Analysis

Fig.2, gives the FTIR result of the zinc oxide nanoparticles. It can be seen that frequency (3447.8cm^{-1}) depict RO-H(Alcohol) wide rounded broad band. The broad band with a very weak intensity of frequency (2374.3cm-1) corresponds to $C \equiv C$) stretch, the broad band 1883.9cm-1 revealed the alkene group, (C = C). The sharp band (1420.1cm-1) corresponds to C = O stretch ketone, R2C = O. The presence of the carbonyl double bond carbon group in the zinc oxide nanoparticles also suggests it to be a good corrosion inhibitor (Lotto et al., 2013).

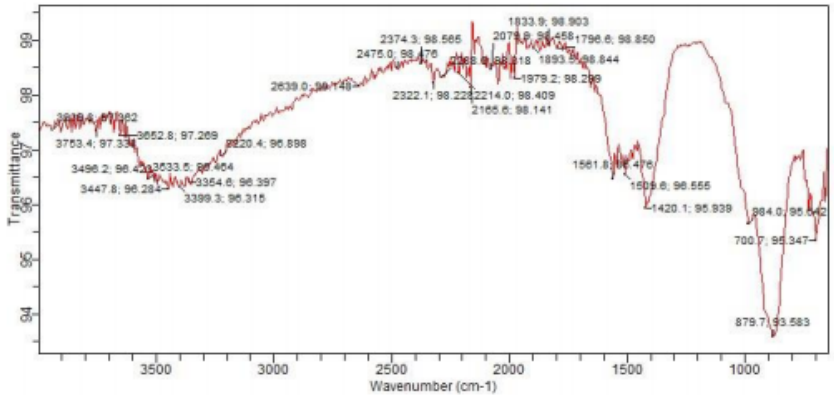

Figure 2: FTIR Spectra for Zinc oxide nanoparticles

Table 2 : Bonds, wave number and intensity of FTIR spectra bond wave number intensity

BOND	WAVE NUMBER	INTENSITY
O – H	3650-3200	Strong, broad
C – H	3300-2700	Medium
N – H	3500-3300	medium, broad
C ≡ H	2260-2220	Medium
C ≡ C	2260-2100	weak-medium
C= C	1680-1600	Medium
C = N	1650-1550	Medium
C = O	1780-1650	Strong
C- O	1250-1050	Strong

(Lotto et al., 2013)

5.3 UV-Visible Spectroscopy

The size of the nanoparticles has a significant impact on how materials' whole properties are altered. In order to investigate the properties of the materials, the size evolution of semiconducting nanoparticles becomes extremely important. The absorption spectrum of ZnO nanopowder is shown in Fig.3, using UV spectroscopy. The band is observed between 230nm to 1000nm of wavelengths, identified as surface plasmon resonance band. The shape of the band indicated a uniform scattering of the nanoparticles due to the excitation of the valence electrons within the nanomaterial. The absorption peak was observed at 571nm.

5.4 Weight loss Analysis

The results of the weight loss method for aluminum in 0.5M, 1.5M, and

2.0M HCl in the absence and presence of varying inhibitor concentrations is shown in Figure 3 – Figure 4. The result obtained shows a higher numerical value of weight loss for blank (absence of inhibitor). Further analysis of the weight loss showed that the sample with the highest concentration of inhibitor had the lowest weight loss, whereas the sample without inhibitor had the highest weight loss. Additionally, Figure 3 – Figure 5, shows that as the concentration of the HCl medium increases, the weight loss also increases, this may be due to the fact that with higher inhibitor concentrations, more molecules are adsorbed on the surface of aluminum metal, covering a wider area of the metal surface and making it more difficult for the electrolyte solution to attack the metal again (Sanni, 2018; Nuru et al., 2016).

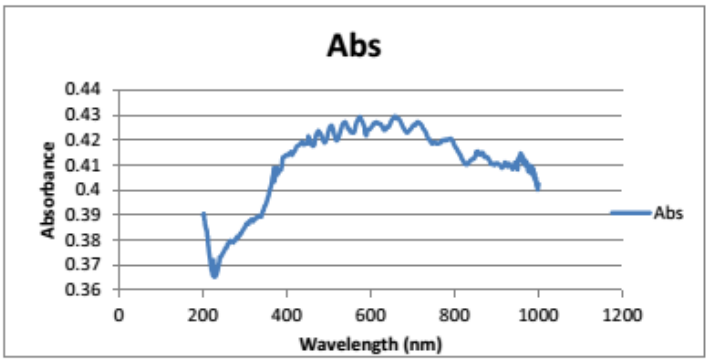

Figure 3: UV-Visible Spectroscopy for ZnO nanopowder

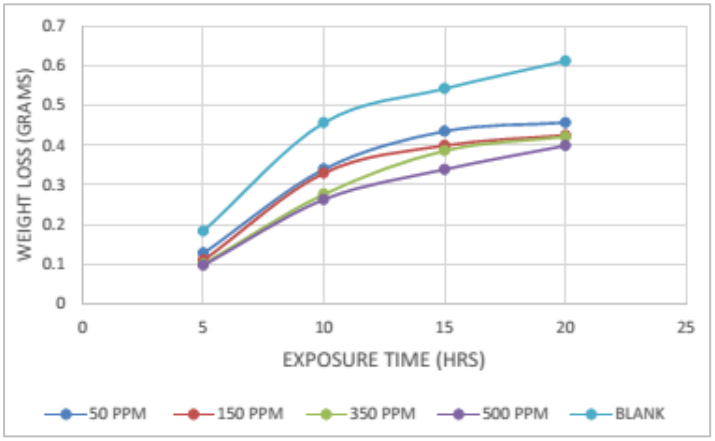

Figure 4: The graph of weight loss against immersion time at room temperature for 0.5 M HCL

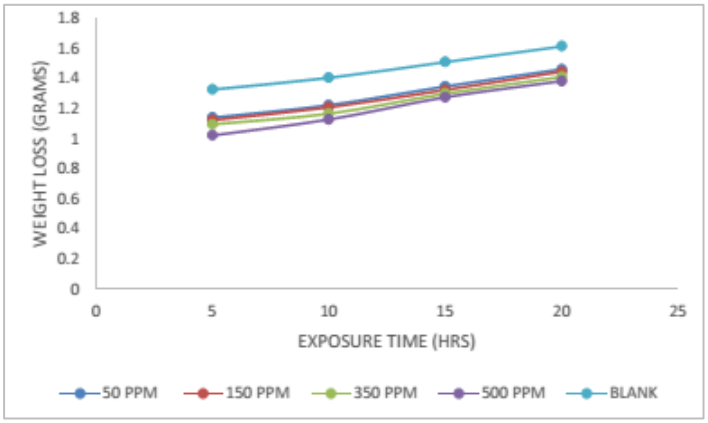

Figure 5: The graph of weight loss against immersion time at room temperature for 1.5 M HCL

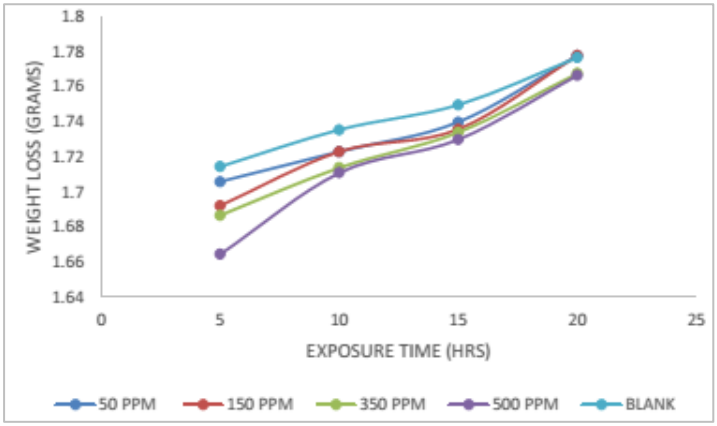

Figure 6: The graph of weight loss against immersion time at room temperature for 2.0 M HCL

5.5 Effect of Inhibitor Efficiency

The inhibition efficiency of the inhibitor against concentration is shown in Figure 6 to Figure 8, for 0.5 M, 1.5 M, 2.0 M of HCl respectively. It was observed that the inhibition efficiency increased with increase in the concentration of inhibitor which resulted in the decrease in corrosion rate. The increase in efficiency may be due to an increase in the amount of inhibitor molecules that are adsorbed on the surface of the aluminum to form a passive layer that protects the metal (Silva et al., 2018). Generally, it has been discovered that inhibitor efficiency decreases with the time of exposure. This phenomenon can be explained by the possibility that, after a longer period of exposure, some of the inhibitor molecules that had previously been adsorbed on the metal surface will partially desorb (Rajeev et al., 2012).

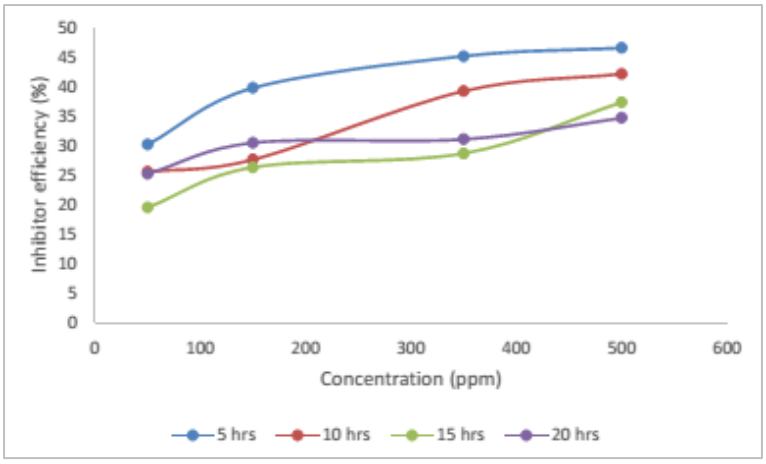

Figure 7: The graph of inhibition efficiency against concentration in 0.5M HCL

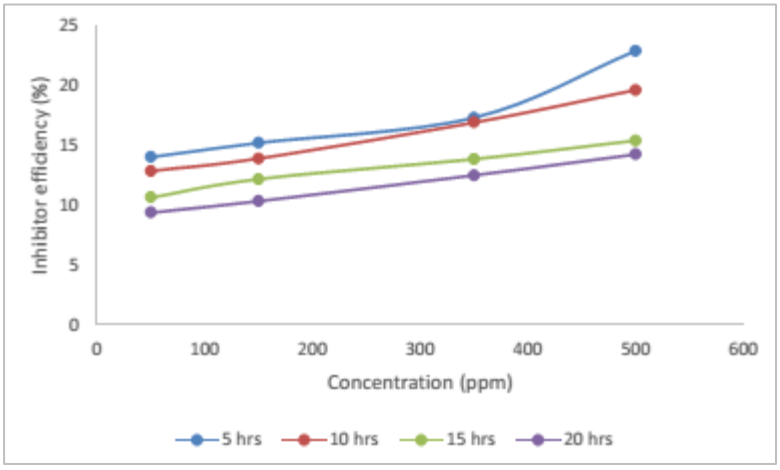

Figure 8: The graph of inhibition efficiency against concentration in 1.5M HCL

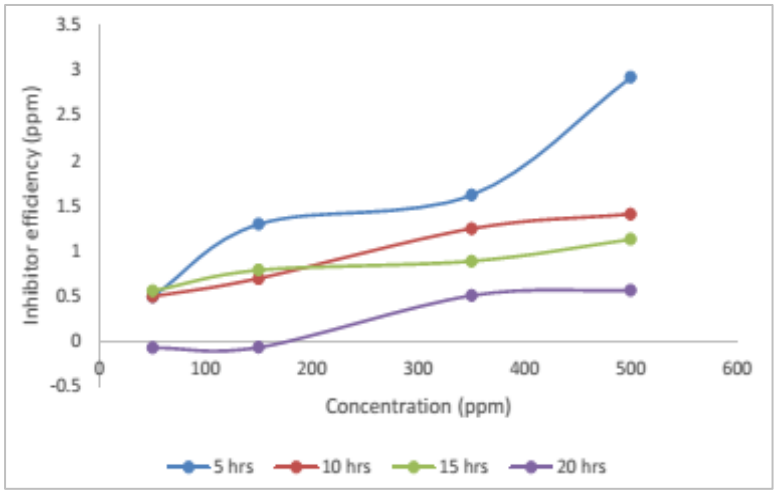

Figure 9: The graph of inhibition efficiency against concentration in 2.0M HCL

5.6 Effect of Surface Coverage

Furthermore, it is discovered that as the concentration of the inhibitor rises, so does the extent of its surface coverage. This shows that an increase in precise concentration increases the number of inhibitor molecules adsorbed on the surface of steel and decreases the amount of surface area that is open to direct attack (Yetri et al., 2015). It can also be seen that comparing Figure 9 to Figure 11, that as the concentration of the HCL medium increases, the surface coverage decreases also. Additionally, the degree of surface protection of the aluminum decreases as exposure time is increased. This may be explained as a result of inhibitor adsorption on the surface of the aluminum coupon and forming a compact protective

thin layer film on the aluminum surface, which lowers the rate of aluminum corrosion in 0.5M, 1.5M and 2.0M HCl solution (Arellanes et al., 2014).

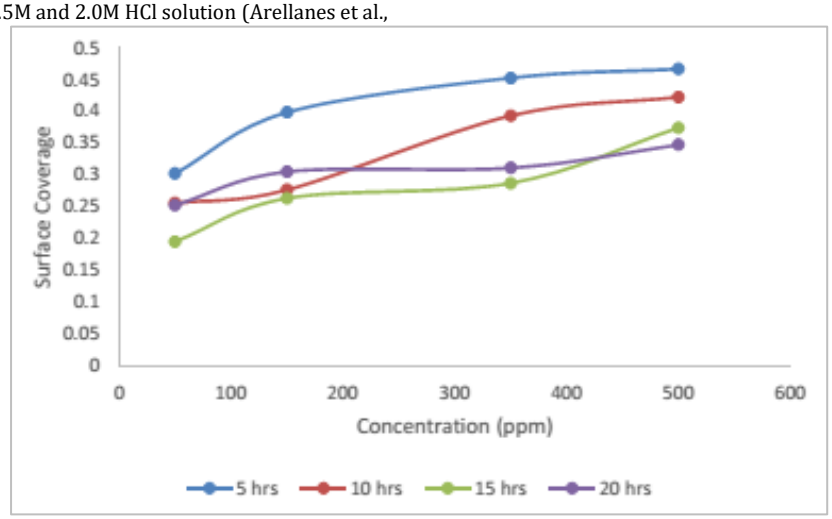

Figure 10: The graph of surface coverage against concentration in 0.5M HCL

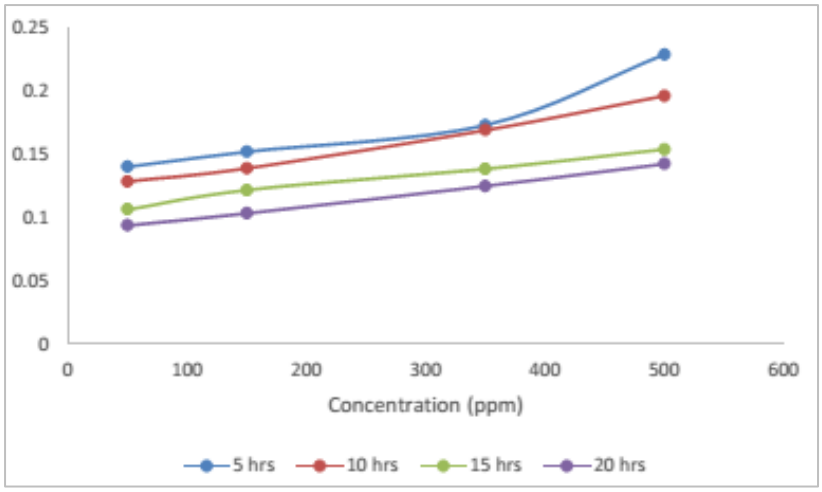

Figure 11: The graph of surface coverage against concentration in 1.5M HCL

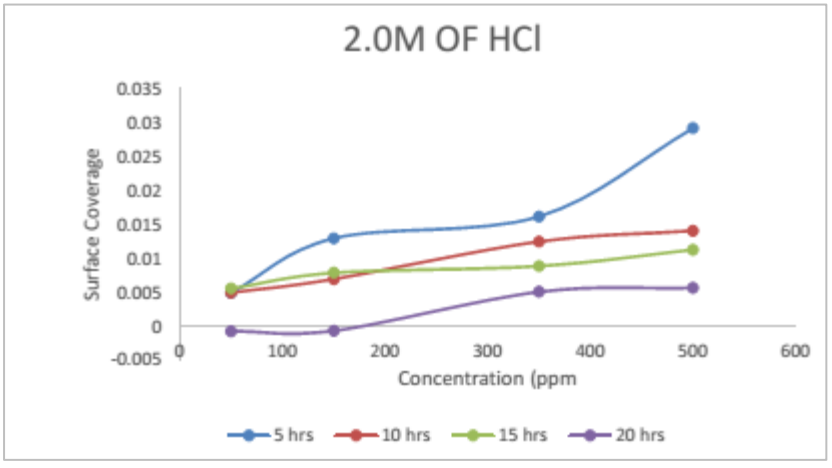

Figure 12: The graph of surface coverage against concentration in 2.0M HCL.

5.7 Effect of Temperature

Figure 12 shows the graph of inhibition efficiency versus temperature (303K, 313K, 323K and 333K) for a fixed immersion time of 2 hours in 0.5 M HCl as presented in Table 3. The results show that the inhibition efficiency of the inhibitor at different concentrations decreases with an increase in temperature, this result supports the mechanism of physical adsorption see Figure 13. This shows that the protective films of the inhibitors formed on the surface of the aluminum metal are less stable at higher temperatures (Abd El-Hameed, 2011).

5.8 Kinetic Activation Energy

Figure 14, shows a plot of the logarithm of corrosion rate against the inverse of temperature which a gives a linear graph with the slope equal to –Ea/2.303R and an intercept equal to log A. From Table 4 it can be seen that the range of values obtained for that of the inhibitors was higher than that of the blank. The reaction is shown to be an endothermic reaction since the activation energy value is higher than the enthalpy value. Higher values of Ea in the presence of inhibitor are a good indication of the inhibitor increasing the energy barrier for the corrosion process. The value for Ea for corrosion of aluminum without inhibitor is 29.60339 KJ/mol, while those with the presence of inhibitor are within the ranges of 35.782 - 38.885 Kj/mol this values indicates that the process of corrosion of aluminum in HCl without inhibitor occurs slower than with inhibitor.

The changes of Ea showed that the inhibitor on the metal surface participate in the adsorption process. Figure 15, shows the plot of log CR/T against inverse of temperature gave a straight line graph with slope equal to -△Ha/2.303R and the intercept equal to {log (R/Nh) + △Sa/2.303R }. The enthalpy of activation (△Ha) and entropy of activation (△Sa) were calculated and tabulated in Table 4. The positive values of enthalpy of activation and negative value of entropy of activation indicates an endothermic reaction and non-spontaneous nature of the reaction respectively. The values of Ea are well observed to be higher than the values △Ha which shows an endothermic reaction.

Table 3: Corrosion rate, Inhibition efficiency at 303-333K at various concentrations of inhibitor at 0.5M HCl

Concentration	303K		313K		323K		333K	
	HE (%)	CR (mm/yr)	IE (%)	CR (mm/yr)	IE (%)	CR (mm/yr)	IE (%)	CR (mm/yr)
50	30.3	104.15	18.7	321.6	272.33	13.7	13.7	448.74
150	39.9	87.79	21.6	310.25	251.24	18.7	18.7	422.59
350	45.3	81.84	44.7	218.59	236.64	27.2	27.2	378.78
500	46.71	79.73	45.7	214.74	198.11	33.9	33.9	343.71
BLANK	0.00	149.49	0.00	395.62	0.00	330.32	0.00	520.125

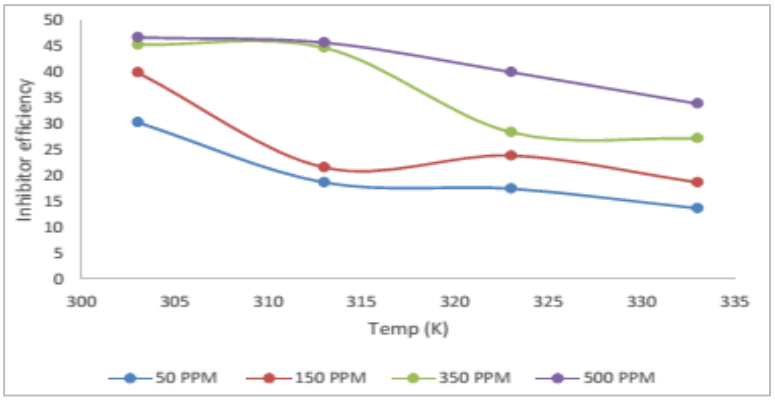

Figure 13: The graph of inhibition efficiency vs temperature at different concentrations of the inhibitor in 0.5M HCL

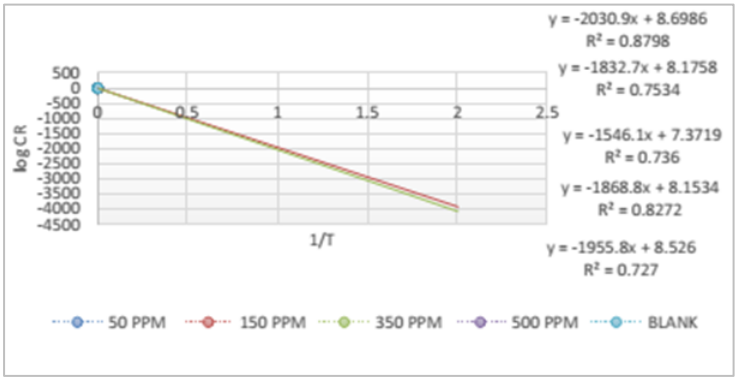

Figure 14: The graph of log CR vs Inverse of temperature at different concentrations of the inhibitor in 0.5M HCL

Table 4: Showing activation energy, enthalpy and entropy at 0.5M HCl

Concentration	Ea (KJ/mol)	ΔH (KJ/mol)	Ea -ΔH	ΔS
50	35.09096	32.43143	2.65953	-97.319
150	37.44798	34.82674	2.62124	-90.451
350	38.88593	33.57260	5.31333	-95.000
500	35.78217	33.15902	2.62315	-97.637
BLANK	29.60339	26.982	2.62124	-112.59

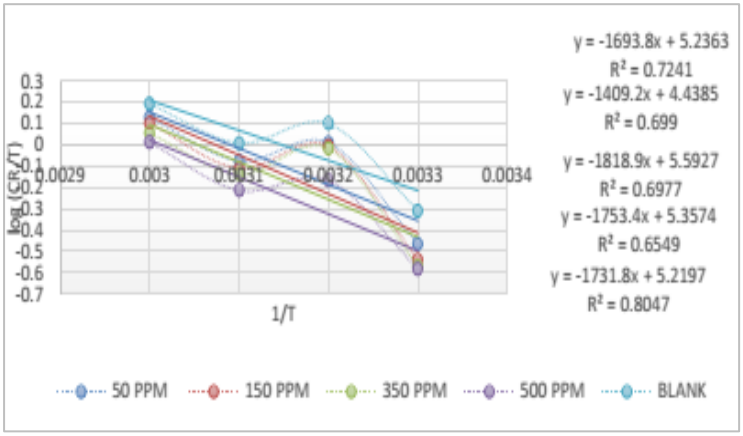

Figure 15: The graph of log (CR/T) vs Inverse of temperature at different concentrations of the inhibitor in 0.5M HCL

5.9 Kinetic Parameter Study

Corrosion rate with respect to inhibitor concentration and exposure time Figure 14 to Figure 15, showed that the corrosion rate with the inhibitor decreases as the inhibitor concentration increases with exposure time showing there is a good indication that the rate of corrosion is reduced. The significant decrease in corrosion rate of aluminum with the inhibitor can be attributed to the adsorption of the inhibitor molecules on the surface of aluminum. The inhibitor molecule acts as physical barrier that restrict the diffusion of ions to and from the aluminum surface which in turn prevent the aluminum atoms (ions) from participating in further anodic or cathodic reactions (redox reaction), hence resulting in decrease in the corrosion rate this corroborates the work of (Buoklah et al., 2006). It is also observed that corrosion rate increased with an increase in the concentrations of acid used as a measure of the corrosive nature of the medium. Figure 13 – Figure 17 shows that the presence of the inhibitor decreased the corrosion rate as inhibitor molecules were adsorbed on the aluminum surface to form a protective film that worked as a barrier that partially prevented ionic interchange; this way, the kinetics of electrochemical reactions are slowed and the corrosion rate on the metal surface is mitigated.

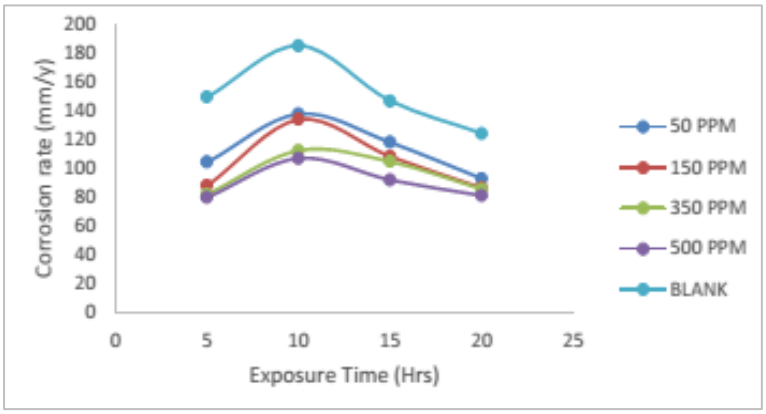

Figure 16: The graph of corrosion rate against time in 0.5M HCL

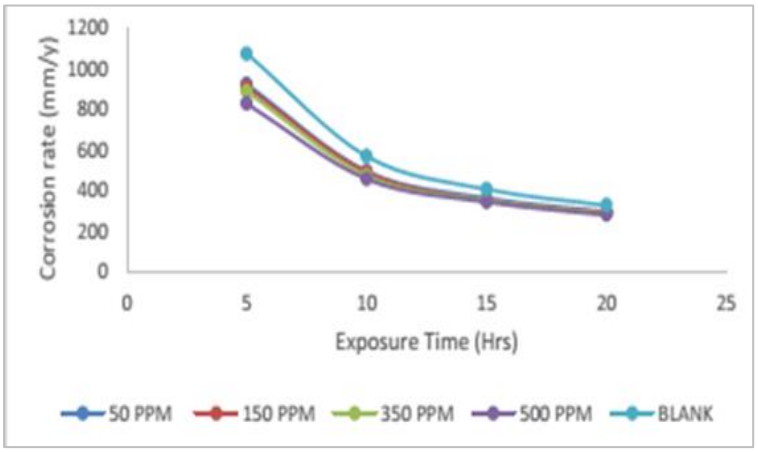

Figure 17: The graph of corrosion rate against time in 1.5M HCL

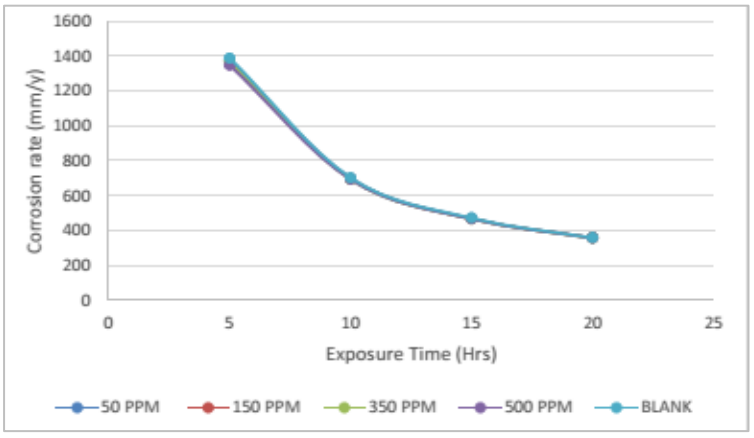

Figure 18: The graph of corrosion rate against time in 2.0 M HCL

5.10 Half-Life Investigation

A Plot of the inverse of the measured weight in grams of the aluminum after and before immersion against time helped to explain the kinetics of the corrosion of aluminum in the acidic media in the absence and presence of inhibitor (El-Ashry et al., 2006; Okafor et al., 2007). Linear plots were obtained as shown in Figure 18 – Figure 19, Mare consistent with first order kinetics and which can also be obtained mathematically from equation 5 (Atkins and Depaula, 2010; Shama and Shama, 2004; Engel and Reid, 2006). The values of the half life constants k obtained from the slope of the plot in Figure 18 to Figure 21 are presented in Table 4 to Table 6. The results obtained indicate that the rate constants decrease with increase in the extracts concentrations from 50ppm to 500ppm (Okafor et al., 2007). If the rate constant doubles, so will the rate of the reaction however, the outcome in this instance indicated a decline in rate constant with increasing concentration, which suggests a potent inhibitor and a

slower rate of corrosion response. Equation 6 was used to derive the half-life values from the rate constant values, and the resulting data is shown in Tables 4 to 6. The half-life values were observed to decrease and increase with increase in concentration of the inhibitor.

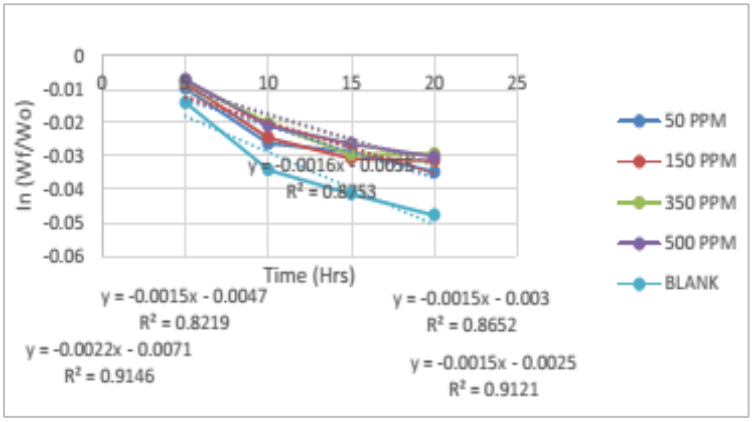

Figure 19: Graph of ln(Wf/Wo) against exposure time with respect to inhibitor concentration in 0.5M.

Table 5: Result of the half-life and R2 values for 0.5 M			
Inhibitor Conc (ppm)	**K(rate constant)**	**$t^{1/2}$ (hrs)**	**R^2**
Blank	0.0022	315.04	0.9146
50	0.0016	433.18	0.8753
150	0.0015	462.07	0.8219
350	0.0015	462.07	0.8652
500	0.0015	462.07	0.9121

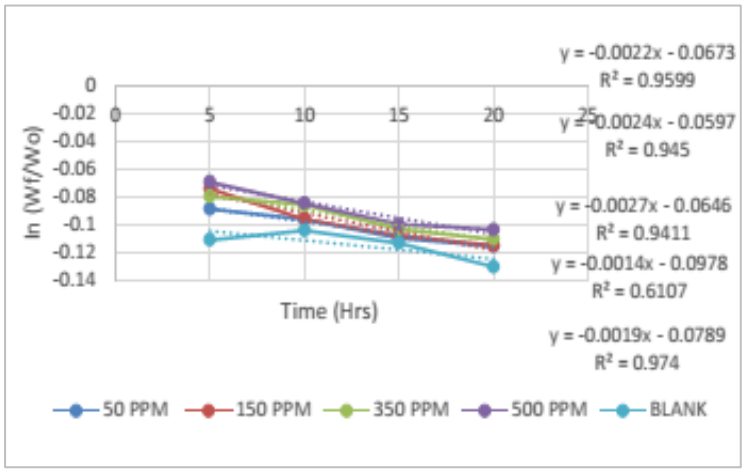

Figure 20: Graph of ln (Wf/Wo) against exposure time with respect to inhibitor concentration in 1.5M

Table 6: Result of the half-life and R2 values for 1.5 M			
Inhibitor Conc (ppm)	**K(rate constant)**	**$t^{1/2}$ (hrs)**	**R^2**
Blank	0.0014	495.07	0.6107
50	0.0019	364.79	0.974
150	0.0027	256.70	0.9411
350	0.0022	315.04	0.9599
500	0.0024	288.79	0.6107

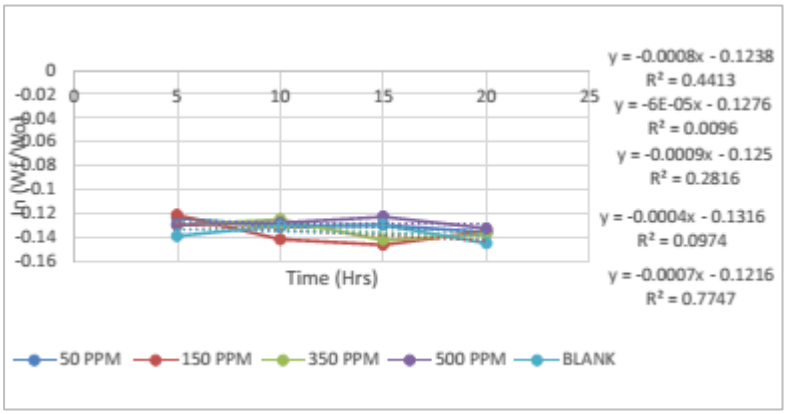

Figure 21: Graph of ln(Wf/Wo) against exposure time with respect to inhibitor concentration in 2.0 M

Table 7: Result of the half-life and R2 values for 2.0 M.

Inhibitor Conc (ppm)	K(rate constant)	$t^{1/2}$ (hrs)	R^2
Blank	0.0004	1732.75	0.0974
50	0.0007	990.14	0.7747
150	0.0009	770.11	0.2816
350	0.0008	866.37	0.4413
500	0.00006	11551.67	0.0096

5.11 Adsorption Isotherms

Adsorption equilibrium is an important information used to study adsorption isotherm process. It shows the relationship between the adsorbate in the liquid phase and the adsorbate adsorbed on the surface of the adsorbent at equilibrium at a particular temperature. The Langmuir, Fruendlich, Temkin and El-Awady isotherms were used to test the experimental data at different temperatures and concentrations.

Table 8: Parameters for different adsorption isotherm at 303K - 333K

Inhibitor	Temp (K)		Langmuir		Fruendlich		Temkin		El Awady	
			K_{ads}	R^2	K_{ads}	R^2	K_{ads}	R^2	K_{ads}	R^2
Zinc oxide nanoparticles with a blend of Musa Paradisiaca	303	0.999	0.1897	0.9718	0.1897	0.9718	0.0721	0.9851	0.3078	0.9815
	313	1.587	0.4319	0.8798	0.4319	0.8798	0.131	0.8539	0.6275	0.86797
	323	2.2432	0.323	0.9247	0.323	0.9247	0.0853	0.848	0.4428	0.8984
	333	2.4213	0.3871	0.9776	0.3871	0.9776	0.0843	0.9291	0.4974	0.9662

5.12 Langmuir Adsorption Isotherm

This adsorption isotherm was carried out on aluminum coupons at various concentrations of Zinc oxide nanoparticles blended with musa paradiasca extract inhibitor at temperatures ranging from 313K – 333K. A plot of C/θ against C is shown in Figure 21, it gives a straight line ($R^2 > 0.9$) which indicates that adsorption follows Langmuir adsorption isotherm. It is observed that as the temperature increases, the value of R squared decreases from 0.9999 to 0.954 which indicates the adsorption of the inhibitor on the aluminum surface obeys Langmuir adsorption isotherm.

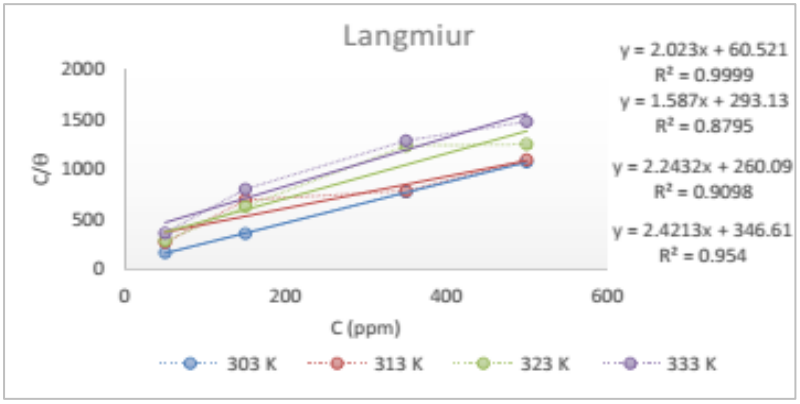

Figure 22: Langmuir adsorption isotherm plot of different temperatures at 0.5 M of HCl

5.13 Fruendlich Adsorption Isotherm

This adsorption isotherm was carried out on aluminum coupons at various concentrations of Zinc oxide nanoparticles blended with musa paradiasca extract inhibitor at temperatures ranging from 313K – 333K. A plot of log θ against log C is shown in Figure 23. The linearity of the graph shows the adsorption of the inhibitors on the aluminum at different concentrations obeys Fruendlich isotherm. The adsorption studies show that the experimental data fitted into the Freundlich isotherm with correlation co-efficient (K_{ads}) greater than 0.90. the adsorption equilibrium constant (K_{ads}) value doesn't exactly show a clear increase or decrease in value as the temperature increases, this may be due to the properties of the aluminum used.

5.14 Temkin Adsorption Isotherm

This adsorption isotherm was carried out on aluminum coupons at various concentrations of Zinc oxide nanoparticles blended with musa paradiasca extract inhibitor at temperatures ranging from 313K – 333K. The isotherm shows the plot of surface coverage (θ) versus the logarithm of the different concentrations of the inhibitor (C), which gives a straight line graph (represented in Figure 24. The values of (K_{ads}) decreased with increase in temperature, which indicates that the adsorption of the inhibitor on the aluminum surface follows Temkin isotherm

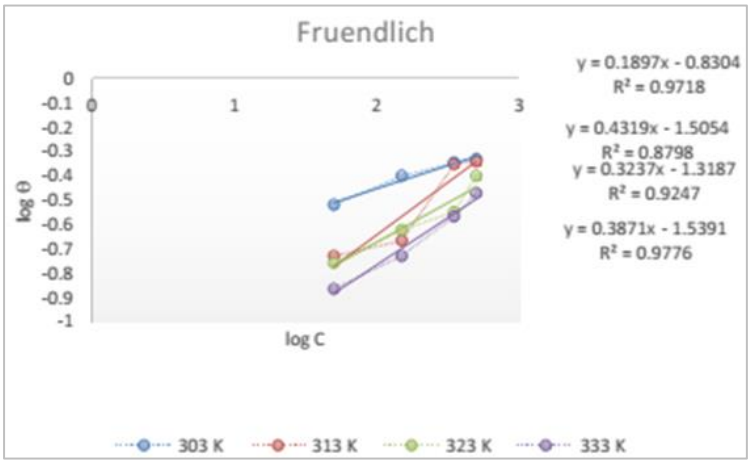

Figure 23: Fruendlich adsorption isotherm plot of different temperatures at 0.5 M of HCl

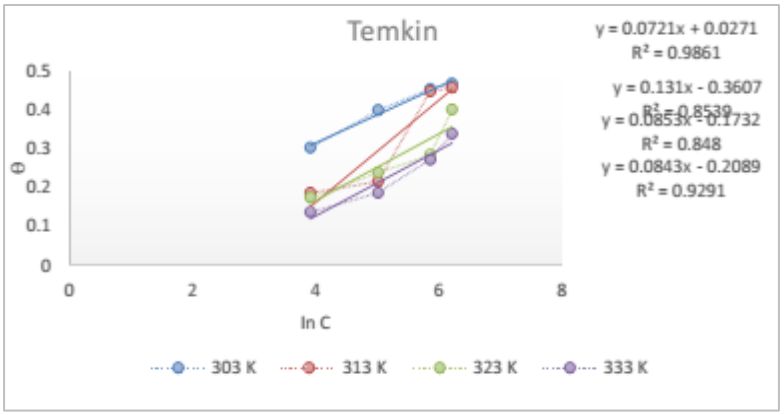

Figure 24: Temkin adsorption isotherm of different temperatures at 0.5 M of HCl

5.15 El Awady Adsorption Isotherm

This adsorption isotherm was carried out on aluminum coupons at various concentrations of Zinc oxide nanoparticles blended with musa paradiasca extract inhibitor at temperatures ranging from 313K – 333K. The characteristics of the isotherm are given by using equation 13. From Figure 25, different concentrations of the inhibitors showed a straight line graph.

The lowest temperature 303 K, gave a straight line graph, it also gave an R squared value higher than 0.9.

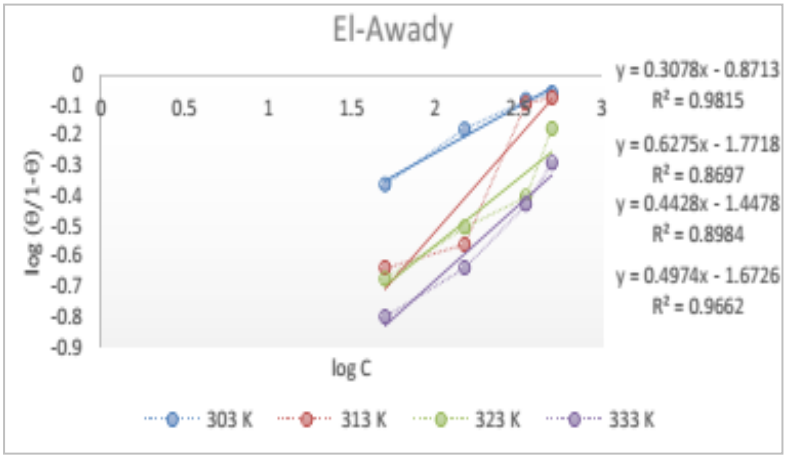

Figure 25: El-Awady adsorption isotherm of different temperatures at 0.5 M of HCl

5.16 Thermodynamic Study

Thermodynamic parameters help in understanding the inhibitive mechanism**.** The free energy of adsorption ΔGads which characterizes the interaction of adsorbed molecules and metal surface, can be calculated with the equation 14

$$\Delta Gads = -RTIn\,(55.5 * K) \quad (14)$$

Where K is the adsorption equilibrium constant, R is the gas constant (8.314 J/mol/K), T is the temperature in kelvin, and 55.5 is the concentration of water in solution expressed in mol/liter (Kahled, 2003).

The negative value of △Gads ensures the adsorption process and stability of the adsorbed layer on the metal surface. This also shows a decrease in the value of △Gads as the temperature increases which is referred to as physical adsorption. Generally, the values of △Gads up to -20KJ/mol are constant with electrostatic interaction between the charged molecules and metals (physisorpton), while those higher than -40 KJ/mol involve sharing or transfer of electrons from the inhibitors to the metal surface to form coordinate type of bond (Chemisorption) (Li et al., 2011). From the experimental data given in Table 8. The calculated values of △G ads was found to be less than -40KJ/mol. The relatively high and negative free energy indicates that a spontaneous adsorption of the inhibitor molecules on the surface of the metal. The enthalpy of adsorption △H ads and entropy of adsorption △S ads were obtained from Gibbs-Helmhotlz

equation as shown in equation 14

$$\Delta G° ads = \Delta H° ads - T\Delta S° ads \quad (15)$$

Figure 26 showed a straight line graph with an intercept of $\triangle H^0$ advertising and a slope of $\triangle S^0$ ads, obtained from plotting $\triangle G^0$ ads versus T. The corrosion mechanism can be inferred from the values of $\triangle H^0$ and $\triangle S^0$ ads. The results for $\triangle H^0$ advertising produced a positive result, indicating that heat is being absorbed and the process is endothermic, confirming the idea that inhibition performance declines with temperature. Thermodynamic characteristics of aluminum adsorption in 0.5M HCl at various temperatures are shown in Table 9.

Table 9: Thermodynamic parameters of adsorption on Aluminum in 0.5M HCl at different temperature

Isotherm	ΔGads (KJ/mol)				ΔH°ads (K/mol)	ΔS°ads (J/mol/K)
	303K	313K	323K	333K		
Langmiur	-11.892	-11.653	-12.955	-13.569	7.6217	-0.0633
Fruendlich	-5.930	-8.267	-7.750	-8.492	15.188	-0.00717
Temkin	-3.493	-5.162	-4.175	-4.271	0.0082	-0.0135
El-Awady	-7.149	-9.239	-8.598	-9.186	8.8516	-0.0547

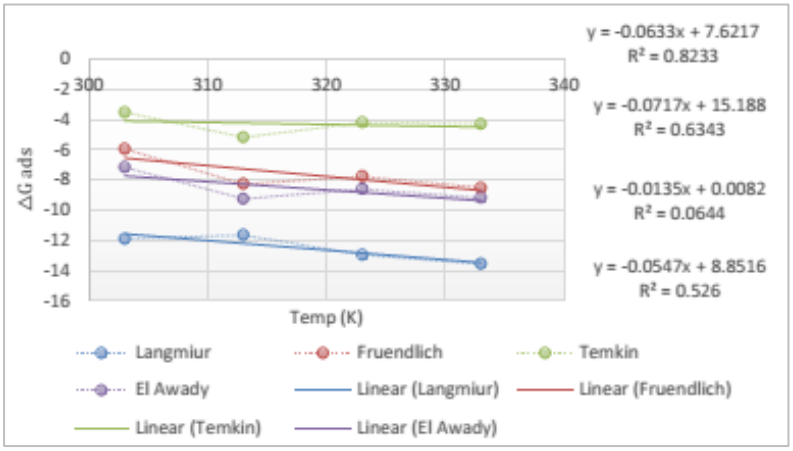

Figure 26: Plot of Gibbs free energy against temperature

6. Conclusion

The presence of flavonoids, saponin, alkaloids, proteins, and tannins in plantain peel extract aided in the bio reduction of zinc acetate to zinc oxide nanoparticles. Gravimetric analysis was used to determine weight loss. The effects of exposure time, inhibitor concentrations, and acid concentrations on weight loss, corrosion rate, inhibition efficiency, and surface coverage on aluminum were investigated. In this study, zinc oxide nanoparticles made from unripe plantain peel were successfully formulated and used as a corrosion inhibitor on aluminum in an acidic medium. The maximum efficiency obtained from the experimental results was 46.70%; this could be explained by the fact that the metal (aluminum) used is highly reactive and forms a thin protective oxide layer that serves as a barrier against further oxidation; the endothermic nature of the reaction is indicated by the positive values of enthalpy of activation and the non-spontaneous nature of the reaction by the negative values of entropy of activation; the spontaneous nature.

Recommendations

This study was conducted using a weight loss strategy. However, additional research on the corrosion process can be conducted using techniques such as linear polarized resistance and electrochemical impedance spectroscopy. It is critical to investigate the optimization of the aluminum metal corrosion process in order to develop model equations for controlling the process. Institutions should have reliable power supplies to ensure precision, repeatability, and accuracy in research.

References

Abd El-hameed, R.S., 2011. Aminolysis of Polyethylene tetrephthalate Waste as Corrosion Inhibitor for Carbon Steel in HCl corrosive medium. Advances in Applied Science Research. II (3), PP. 483-499.

Bedair, M.A., Metwally, M.S., Soliman, S.A., Al-Sabagh, A.M., Salem, A.M., Mohamed, T.A., 2015. Extracts of Mint and Tea as Green Corrosion Inhibitors for Mild Steel in Hydrochloic acid solution. Al Azhar Bul. Sci., 26, Pp. 1–14.

Chaubey, N., Singh, V.K., Quraishi, M.A., 2017. Electrochemical approach of Kalmegh leaf extract on the corrosion behavior of aluminium alloy in alkaline solution. Int. J. Ind. Chem., 8, Pp. 75–82.

Elemike, E.E., Onwudiwe, D.C., and Mbonu, J.I., 2021. Facile synthesis of cellulose–ZnOhybrid nanocomposite using Hibiscus rosa-sinensis leaf extract and their antibacterial activities. Applied Nanoscience, 11 (4), Pp. 1349–1358. https://doi.org/10.1007/s13.

El-Etre, A., 2003. Inhibition of aluminum corrosion using Opuntia extract. Corros. Sci., 45, Pp. 2485–2495.

Ennouri, A., Lamiri, A., Essahli, M., 2017. Corrosion Inhibition of Aluminium in Acidic Media\ by Different Extracts of Trigonellafoenumgraecum L Seeds. Port. Electrochim. Acta, 35, Pp. 279.

Haley, T.J., 1965. Pharmacology and toxicology of the rare earth elements. J. Pharm. Sci, 54, Pp. 663–67.

Imade, E.E., Ajiboye, T.O., Fadiji, A.E., Onwudiwe, D.C., Babalola, O.O., 2022. Green synthesis of zinc oxide nanoparticles using plantain peel extracts and the evaluation of their antibacterial activity. Scientific African, 16, Pp. e01152.

Mhammedi, M.A., Chaini, A., 2007. Investigation of the inhibitive effect of pyrazolo [3, 4-b] pyridine on corrosion of stainless steel in 1 M HCl solutions. Leonardo El J. Pract. Technol., 11, Pp. 37-46.

Muller, B., 2002. Corrosion inhibition of aluminium and zinc pigments by saccharides. Corros. Sci., Pp. 1583–1591.

Namrata, C., Vinod, K.S., Quraishi, M.A., 2015. Effect of some peel extracts on the corrosion behavior of aluminum alloy in alkaline medium. Int J. Ind Chem., 6, Pp. 317–328. DOI 10.1007/s40090-015-0054-8

Oguzie, E.E., 2005. Corrosion inhibition of mild steel in hydrochloric acid solution by methylene blue dye. Mater. Lett., 59, Pp. 1076–1079.

Oguzie, E.E., Onuoha, G.N., Onuchukwu, A.I., 2005. The inhibition of aluminium corrosion in potassium hydroxide by "Congo Red" dye, and synergistic action with halide ions. Anti Corros. Methods. Mater., 52, Pp. 293–298.

Okafor, P.C., Ebenso, E.E., Ekpe, U.J., 2010. Azadirachta indica Extracts as Corrosion Inhibitor for Mild Steel in Acid Medium. Int. J. Electrochem. Sci., 5, Pp. 978–993.

Raghavendra, N., Bhat, J.I., 2018. Anti-corrosion properties of areca palm leaf extract on aluminum in 0.5 M HCl. S. Afr. J. Chem., 71, Pp. 30–38.

Ryl, J., Wysocka, J., Cieslik, M., Gerengi, H., Ossowski, T., Krakowiak, S., Niedzialkowski, P., 2019. Understanding the origin of high corrosion inhibition efficiency of bee products towards aluminium alloys in alkaline environments. Electrochim. Acta, Pp. 3.

Tarek, A.Y., Rageh, K.H., Abdulrahman, G.A., Ahmed, T.A.M.B.A., and Mortaga, M.K., 2022. Environment-Friendly Corrosion Inhibitors for Aluminum in Hydrochloric Acid: Quantum and Experimental Research

Xhanari, K., Finsgar, M., Knez, H.M., Maver, U., Knez, Z., Seiti, B., 2017. Green corrosion inhibitors for aluminium and its alloys. RSC Adv., 7, Pp. 27299–2733.